CHEMBIOCHEM

DOI: 10.1002/cbic.200800721

NO Formation by Neuronal NO-Synthase can be Controlled by Ultrafast Electron Injection from a Nanotrigger

Edward Beaumont,[a] Jean-Christophe Lambry,[a] Mireille Blanchard-Desce,[c] Pavel Martasek,[d] Satya P. Panda,[e] Ernst E. H. van Faassen,[f] Jean-Claude Brochon,[g] Eric Deprez,[g] and Anny Slama-Schwok*[a, b]

Nitric oxide synthases (NOSs) are unique flavohemoproteins with various roles in mammalian physiology. Constitutive NOS catalysis is initiated by fast hydride transfer from NADPH, followed by slower structural rearrangements. We used a photoactive nanotrigger (NT) to study the initial electron transfer to FAD in native neuronal NOS (nNOS) catalysis. Molecular modeling and fluorescence spectroscopy showed that selective NT binding to NADPH sites close to FAD is able to override Phe1395 regulation. Ultrafast injection of electrons into the protein electron pathway by NT photoactivation through the use of a femtosecond laser pulse is thus possible. We show that calmodulin, required for NO synthesis by constitutive NOS, strongly promotes intramolecular electron flow (6.2-fold stimulation) by a mechanism involving proton transfer to the reduced FAD^{-} site. Site-directed mutagenesis using the S1176A and S1176T mutants of nNOS supports this hypothesis. The NT synchronized the initiation of flavoenzyme catalysis, leading to the formation of NO, as detected by EPR. This NT is thus promising for time-resolved X-ray and other cellular applications.

Introduction

NOS catalysis is initiated by the combined transfer of electrons and a proton from NADPH to the flavin FAD located in the reductase domain of the enzyme. This reductase domain closely resembles mammalian cytochrome P450 reductase.[1–3] It catalyzes the oxidation of NADPH and reduction of FAD, with subsequent electron transfer to the second flavin FMN (Scheme 1).[1–2] Calmodulin (CaM) binding at high Ca^{II} concentrations mediates electron transfer (ET) flow between the heme (subunit B) and reductase domains (subunit A).[4–5] Calmodulin binding is thought to induce structural rearrangements required for catalysis and is an absolute requisite for NO formation from constitutive NOS, endothelial NOS (eNOS), and neuronal NOS (nNOS).[6–7] These enzymes generate the low concentrations of NO used in signaling pathways to regulate blood flow and pressure, neuronal development, and neurotransmission.

The structural parameters affecting electron flow in NOS have mostly been deduced from indirect measurements with external electron acceptors, such as cytochrome c or ferricyanide, that were generally based on stopped-flow techniques.[6–12] At least two different conformational rearrangements have been shown to impede electron flow in NOS. This slows catalysis by NOS enzymes, as a single fully activated nNOS dimer releases only about a hundred NO molecules per minute.[1–2] In the X-ray structure of the nNOS reductase domain, FAD access to nicotinamide (Nic) is blocked by the stacking of Phe1395 on FAD; this results in a conformation that is inactive for catalysis.[9]

The first slow conformationally gated process, which initiates catalysis through the transfer of a hydride (that is, two electrons and a proton) from NADPH to the flavin FAD, is controlled by a phenylalanine residue—Phe1395.[13–14] This regulatory residue, located between NADPH and FAD, is moved away from FAD by a concerted rotation of the Nic moiety to yield

[a] *E. Beaumont, J.-C. Lambry, A. Slama-Schwok*
Unité INSERM 696, Laboratory for Optics and Biosciences
Ecole Polytechnique
91128 Palaiseau (France)

[b] *A. Slama-Schwok*
Virologie et Immunologie Moléculaires, INRA UR892
Domaine de Vilvert, 78352 Jouy en Josas (France)

[c] *M. Blanchard-Desce*
Photonique Moléculaire, UMR CNRS 6510, Université de Rennes I
Campus de Beaulieu, 35042 Rennes (France)

[d] *P. Martasek*
Department of Pediatrics and Center for Applied Genomics
First School of Medicine
Charles University of Prague
12808 Prague (Czech Republic)

[e] *S. P. Panda*
Department of Biochemistry, University of Texas Health Science Center
San Antonio, TX 78229-3900 (USA)

[f] *E. E. H. van Faassen*
Debye Institute, Section Interface Physics, Utrecht University
Princetonplein 1, 3508TA, Utrecht (The Netherlands)

[g] *J.-C. Brochon, E. Deprez*
LBPA, CNRS UMR 8113, Ecole Normale Supérieure de Cachan
61 av. du Président Wilson, 94235 Cachan (France)

Supporting information for this article is available on the WWW under http://dx.doi.org/10.1002/cbic.200800721.

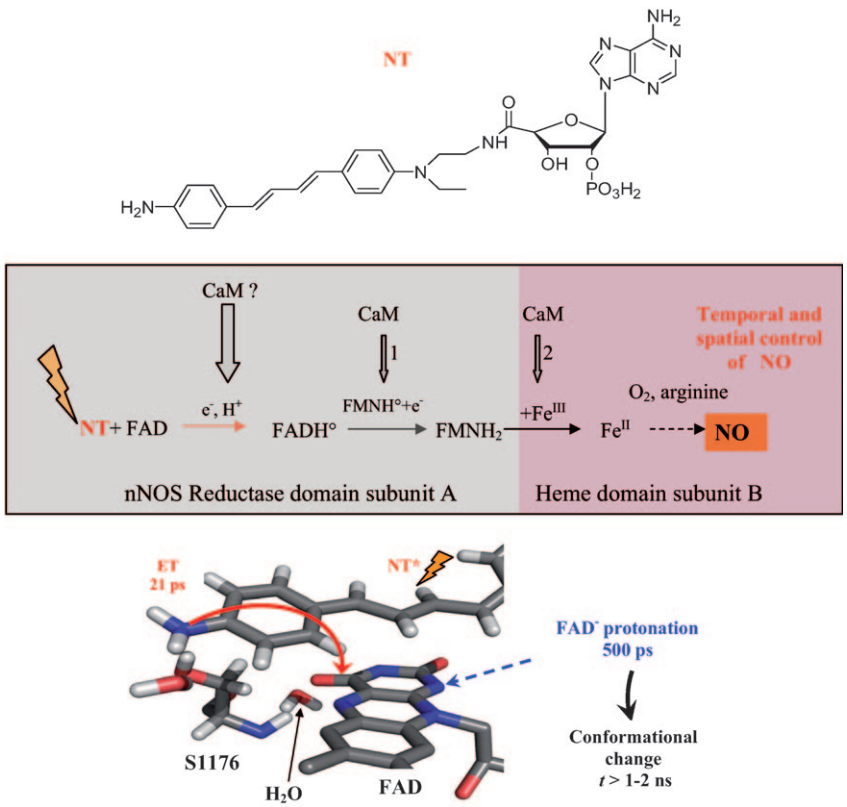

Scheme 1. Upper panel: chemical structure of the NT; this compound should control NO formation with high spatial and temporal accuracy.[17,24] Middle panel: schematic diagram of electron flow in nNOS from the NT to the final NO product, highlighting the proposed (thick vertical arrow) and known influence of Ca^{II}/calmodulin binding on catalysis (arrows 1 and 2). Replacement of NADPH by the NT, which can be activated by light, leading to electron transfer to FAD, and up to the formation of NO, was studied here and is highlighted in red. This scheme does not detail all the steps in nNOS catalysis. Bottom panel: mechanistic hypothesis relating to the initiation steps of nNOS catalysis in the presence of NT and Ca^{II}/calmodulin, as deduced from ultrafast kinetics and molecular modeling.

the active conformation of NADPH. A second slow gating process involves the FMN module. This conformational change is thought to involve FMN domain mobility, which is triggered by Ca^{II}/calmodulin binding, and increases the rate of electron transfer between FMN and heme.[7,9,15–16] The reductase domain thus donates electrons to cytochrome c more efficiently in the presence of calmodulin. It has been suggested that NADPH binding represses the calmodulin activation of electron transfer in nNOS.[6]

According to recent models, NADPH binding locks the enzyme in a "closed state," in which the FMN module is closely associated with the FAD–NADPH binding domains.[9,15] In this state, electrons can be passed from FAD to FMN but not to outside electron acceptors such as cytochrome c. The "open state," in which effective electron transfer from FMN to the heme can take place, is facilitated by a major movement of the FMN module; this was first suggested by the X-ray structure.[9] CaM accelerates this conformational change. Two regulatory elements are involved in this conformational change from the closed to the open states: the C-terminal tail, which lies at the interface between the FMN module, and the FAD subdomain and the autoregulatory region in the FMN subdomain in concerted interactions with calmodulin.[7] Key regulatory amino acids in the vicinity of NADPH and FAD include Ser1176, Asp1393, and Phe1395 (the "catalytic triad") in nNOS.[8–14] Mutations in which the Ser1176 residue is replaced by an Ala residue show decreased rates of reduction of electron acceptors (for example, ferricyanide or nNOS flavin) by 20-fold. Interestingly, the effect of calmodulin on nNOS activity was strongly attenuated by this mutation.[12] Similarly, the replacement of Asp1393 by a Val residue abolished the effect of Ca^{II}/calmodulin on the rate of reduction of nNOS flavin.[11]

Such conformational gating processes are often several orders of magnitude slower than electron transfer rates in proteins.[3] The spectroscopic effects of CaM binding to nNOS on electron transfer may therefore be masked by upstream rearrangements near the flavin domain. We recently designed a nanotrigger (NT) for synchronized electron injection into FAD flavin to initiate NOS catalysis with light within 110 ps after a laser pulse[17] (Scheme 1). The binding characteristics of the trigger are very similar to those of true NADPH, and the trigger binds competitively to the NADPH site at concentrations in the micromolar range.[17]

We used this NT to unravel the processes of intramolecular electron transfer and structural rearrangements in the full-length native nNOS. In particular, we studied the effect of calmodulin on the initial stage of the catalytic cycle (Scheme 1). By NO spin trapping, we showed that photoactivation of the NT promoted nNOS catalysis, leading to formation of the final product—NO—thereby demonstrating the relevance of the NT as a nonperturbing mechanistic tool for studies of electron transfer events.

The selective binding of the NT to nNOS was assessed by fluorescence measurements and molecular modeling. As would be expected from the design and the reported interactions of NADPH with Arg1400,[9,18–19] NT was selectively targeted to the NADPH sites of nNOS. Molecular modeling revealed that the regulatory Phe1395 flipped away from FAD upon NT binding.[13–14] In this complex, the photoactive moiety of NT was located 5.3 ± 0.5 Å from the FAD acceptor. Simulations demonstrated similarities between the active form of NADPH and NT, so the NT was probably probing an environment similar to that probed by the active NADPH in the nNOS enzyme.

In this active conformation of the enzyme with FAD accessible to bound NT, electron transfer from NT* to FAD took place in 110 ps in the absence of calmodulin and in 20 ps in the presence of calmodulin, as shown by ultrafast pump-probe experiments. Calmodulin binding decreased the observed rate of charge recombination from the reduced FAD to the oxidized NT species, thus enhancing the net electron transfer yield in nNOS by a factor of 6.2. Our first direct measurement of ET rates revealed that calmodulin promoted electron flow between NADPH and FAD, as previously suggested.[20] Scheme 1 presents the main steps in nNOS catalysis, highlighting the known regulation of these steps by calmodulin[7,12–16,20–23] and the proposed effect of this cofactor as judged from the results of this study. Experiments on the Ser1176Ala and Ser1176Thr point-mutants of nNOS confirmed that the Ser1176 residue is probably directly involved in the action of CaM, together with its H-bonding partners. The close proximity of Ser1176 both to the NT and to FAD shown by molecular modeling may account for the role of this residue in regulating the first catalytic step, possibly by promoting FAD^- protonation, thereby decreasing the rate of charge recombination.

Results

NT specifically binds to the NADPH binding sites of nNOS as shown by fluorescence spectroscopy and molecular modeling

The selective addressing of the NT to NADPH sites within the reductase domain of the endothelial NOS enzyme has previously been demonstrated in stopped-flow experiments.[17] NT binding reduced the rates of NADPH oxidation and flavin reduction by competing with NADPH binding in the eNOS reductase domain. These competition experiments thus demonstrated the specific targeting of NT to the NADPH sites.[17] Evidence for NT binding to full length WT nNOS was provided by large changes in flavin fluorescence (Figure 1). The emission spectrum of nNOS was characterized by a maximum at 520 nm (upon excitation at 420 nm), corresponding to flavin fluorescence (**1** or **6** in Figure 1 A). The binding of NT to nNOS gave rise to a characteristic emission mode at 465 nm (**6** to **7**, arrow; see also the differential spectrum **8**), which is similar to that observed in response to $NADP^+$ binding upon excitation at 420 nm (**1** to **2**, arrow; see also the differential spectrum **3**). However, the increase in fluorescence intensity induced by the NT was much greater than that promoted by $NADP^+$ binding (compare **7** and **9** with **6**). Under these conditions, the intrinsic fluorescence of NT was characterized by a maximum at 520 nm, whereas $NADP^+$ fluorescence was negligible (see **10** and **5**, respectively). In contrast with the disruptive effect of calmodulin on the nNOS·$NADP^+$ complex (**2** to **4**, arrow), the emission of the NOS·NT complex at 465 nm was significantly enhanced by the presence of calmodulin (**7** to **11**, arrow; see also the differential spectrum **12**); this suggests that this complex remains stable upon calmodulin binding. Similar results were obtained on direct flavin excitation at 450 nm (Figure 1 B): NT binding to nNOS enhanced the fluorescence emission at 520 nm by a factor of 1.5 (**13** to **14**, arrow). A substantial decrease in flavin fluorescence induced by $NADP^+$ binding in the presence of CaM has been reported and was attributed to $NADP^+$ affecting the local environment of FMN.[16] Fluorescence levels observed with AMP were 45% lower than those

λ_{exc} (nm)/ PM (V)	nNOS alone 8 μM	+ $NADP^+$ 40 μM	+ NT 5 μM	+ $NADP^+$ 40 μM + CaM 6 μM	+ NT 5 μM + CaM 6 μM
420/ 750	**1**	**2**		**4**	
420/ 650	**6**	**9**	**7**		**11**
450/ 750	**13**		**14**		**15**

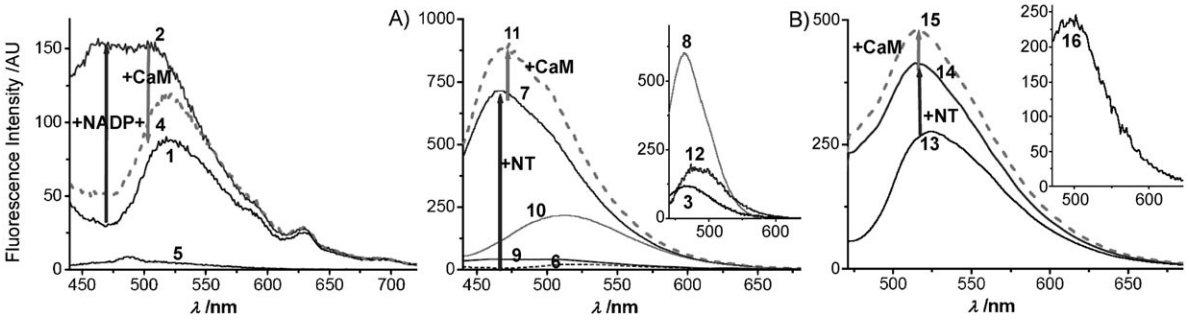

Figure 1. Effect of CaM on the steady-state fluorescence of NT-bound nNOS and of nNOS with excess $NADP^+$. The fluorescence emission spectra were recorded as described in the Experimental Section at A) $\lambda_{ex}=420$ nm or at B) $\lambda_{ex}=450$ nm, numbered **1**–**16** as detailed in the chart above. **3** A) inset: differential spectrum (**2**−**1**); **5**) $NADP^+$ alone. **8** A) inset: differential spectrum (**7**−**6**). **10**) NT alone. **12**) A) inset: differential spectrum (**11**−**7**). **16**) B) inset: differential spectrum (**15**−**14**). [NOHA] = 80 μM = [BH_4]. Figure 1 A compares $NADP^+$ binding to nNOS (left panel) with NT binding to nNOS (right panel); $NADP^+$ and NT induced similar qualitative changes. After direct flavin excitation at 450 nm (Figure 1 B), NT binding to nNOS enhanced the fluorescence emission at 520 nm by a factor of two (**13** and **14**) whereas emission increased by 32% in $NADP^+$·nNOS (data not shown). As shown in experiments with excitation at 420 nm, calmodulin enhanced the fluorescence intensity of the NOS·NT complex (compare **14** and **15** in Figure 1 B and see **16** (inset)).

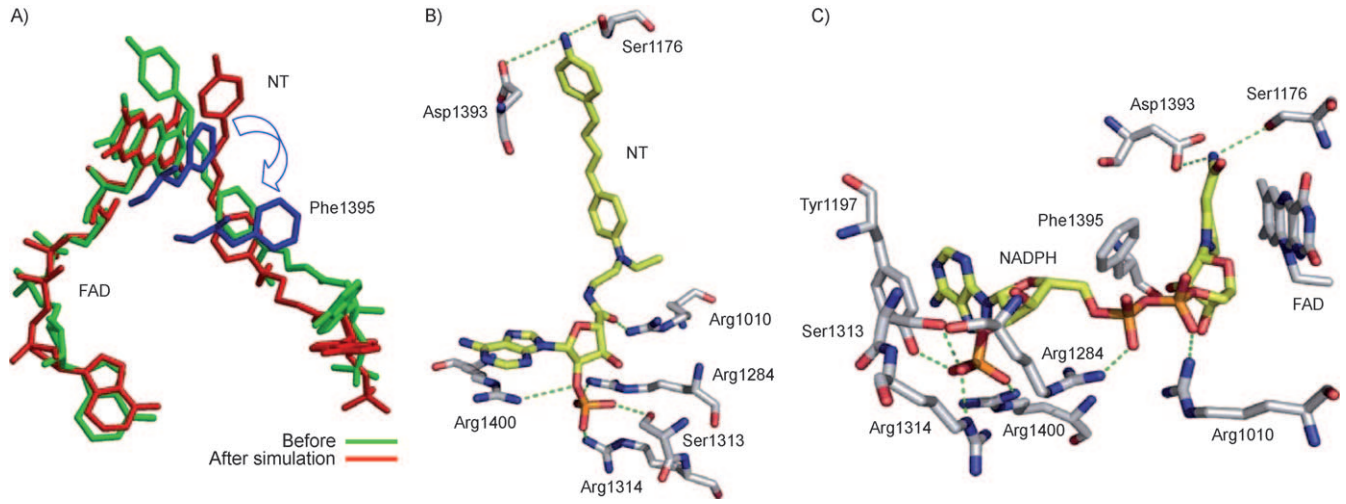

Figure 2. Docking of NT into the nNOS reductase domain (1TLL) by molecular modeling. A) Comparison of the structures before (green) and after the simulation protocol (red) detailed in the Experimental section; note the large tilt of Phe1395, shown in blue and emphasized by the arrow, bringing NT closer to FAD isoalloxazine rings. B) Details of the interactions of NT with nNOS in the NADPH site: note the multiple H-bonds through arginine residues at the nucleotidic edge of NT and interactions through the terminal amino groups in close proximity to the regulatory Ser1176 and Asp1393 residues. C) Very similar H-bonding interactions are experienced by active NADP(H) in the same site of nNOS, through Arg1400, Ser1313, Arg1314, Arg1284, and Arg1010, with additional stacking of the adenine ring through a Tyr residue.[9]

observed with $NADP^+$; this is in contrast with what we observed with the NT, probably reflecting a looser complex with AMP than with $NADP^+$.[16]

Molecular modeling was used to characterize the interactions of the bound NT with nNOS further and to compare it with NADPH. NT was docked by replacing the natural cofactor in the NADP(H)-containing structure of the nNOS reductase domain (1TLL).[9] A high-temperature simulation protocol was used to disrupt weak interactions in order to reach an equilibrium structure rapidly. This required construction of the missing fragments from the X-ray structure (see Experimental). Figure 2A shows the structural differences observed before and after the heating and equilibration phases, mimicking NT binding to nNOS. Significantly, Phe1395 rotated away from FAD after equilibration (arrow). This flip released the Phe1395 stacked on FAD, bringing NT and FAD into close proximity. In all simulations, NT binding induced the rotation of Phe1395 away from FAD, even when small fluctuations from the stable complex presented in Figure 2 occurred. The distance between N5 of FAD and N (from the terminal NH_2) of NT was 5.3 ± 0.5 Å, a short enough distance for efficient electron transfer (Figure 2A).

As a reference for NT binding, simulations were also performed with the native NADPH cofactor to mimic the conformational change required to initiate catalysis in silico. The first steps of the transition between inactive and active forms of NADPH were characterized by a rotation of the Nic moiety of NADPH (shown in a movie provided in the Supporting Information). The Phe1395 flip was not observed after simulation for 1.5 ns at 400 K; this suggests that this step is driven by a high energy barrier regulating the ratio between stacked and unstacked (on FAD) conformations. The NT cannot follow a motion with amplitude as large as that for the flexible Nic moiety of NADPH. Indeed, the conjugated chain of the NT was always found in an extended conformation, rigid enough to prevent large rotations. Figures 2B and C compare the NT and active NADPH at the NADPH site of nNOS. The active form of the NADPH cofactor was obtained by constraining the NADPH Nic moiety to be inserted between FAD and Phe1395 at the starting point before the 400 K simulation protocol. In its active form, the distance between N5 of FAD and the hydride-donating carbon of NADPH was reduced to $d = 4.0 \pm 0.5$ Å (Figure 2C) from $d = 13.0 \pm 0.5$ Å in the inactive form.[9]

Bound NT was stabilized by a number of hydrogen bonds (Figure 2B). The terminal phosphate group of NT was H-bonded—with Arg1400, Arg1314, and Arg1284 in particular—demonstrating similar recognition of the nucleotidic part to that seen with NADPH, as would be expected from the design (Figure 2C).[17,24] The electrostatic binding energy difference was similar: $\Delta E \approx -500$ kcal mol^{-1} for active NADPH and NT. The amide carbonyl oxygen of NT was H-bonded to Arg1010, as an alternative to the H-bond to one of the phosphate group of NADPH. Additional H-bonding such as that between the terminal amino group and Asp1393 and Ser1176 stabilized the complex further. Ser1176 was shown to be important for electron transfer;[8–12] it is only 3 Å from FAD and is also close to the potential proton donors His1032, water molecules, and Cys1349. This residue may therefore be involved in a putative proton transfer to FAD^-, as confirmed below by our transient data. The H-bonding interactions of NT and active NADPH with protein were quantified by van der Waals energy differences: $\Delta E_{vdW} = -67.8 \pm 2.5$ and -56.9 ± 5.1 kcal mol^{-1}, respectively. Thus, NT was somewhat more strongly stabilized than active NADPH in the NADPH binding site through hydrogen bonds and probably probed a similar protein environment within the NADPH site.

Photoexcitation of NT triggered the catalytic cycle of NOS—EPR detection of NO

NOS catalysis involves two consecutive reactions, beginning with the substrate L-arginine, and passing through the *N*-hydroxyarginine (NOHA) intermediate to the citrulline and NO products at the heme site. We investigated whether NT specific binding would trigger the electron flow associated with NOS catalysis and yield NO after light excitation, by carrying out steady-state irradiation experiments at $\lambda = 400 \pm 30$ nm in an aerated solution of nNOS. After ten minutes of illumination, Fe·MGD was added, and an aliquot was collected and snap-frozen in liquid nitrogen. The yield of nitrosylated Fe·MGD complexes was determined by EPR, by comparison of the sample with calibrated reference solutions of NO·Fe^{II}·MGD (25 μM). Aliquots were expected to contain a mixture of ferrous and ferric nitrosyl complexes. Only the ferrous form is paramagnetic and detectable by EPR. Each aliquot was therefore analyzed twice: as taken, and after reduction with dithionite. Upon reduction the color of the solution changed from brownish to a greenish hue. EPR spectra confirmed that the unreduced aliquot contained $\approx 50 \pm 7$ pmol of paramagnetic NO·Fe^{II}·MGD complexes (data not shown). Reduction with dithionite (50 mM) increased the quantity of NO·Fe^{II}·MGD to 300 ± 50 pmol. The greenish hue of the reduced solution may be attributed to the intense green color of the ferrous NO·Fe^{II}·MGD complex. Figure 3A shows an EPR spectrum of a frozen aliquot after reduction with dithionite. The triplet hyperfine structure near $g = 2.035$ is characteristic of nitrosylated iron dithiocarbamate complexes, such as NO·Fe^{II}·MGD.[25] No EPR signal was obtained under identical conditions if nNOS was omitted (Figure 3B) or if the solution was kept in the dark (Figure 3C). For reference, we also determined the normal enzymatic activity of nNOS after addition of NADPH (0.3 mM) in the absence of light and NT (subsequently reduced with dithionite). In this case, the normal catalytic cycle of nNOS (5 μM) resulted in the formation of NO·Fe^{II}·MGD (100 ± 15 pmol).

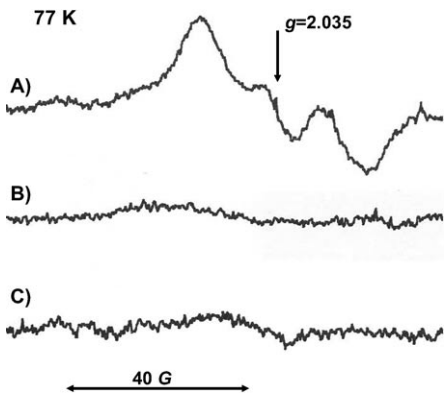

Figure 3. EPR absorption spectrum of the Fe^{II}·MGD·NO adducts obtained after light irradiation of NT bound to nNOS. The Fe·MGD complexes were injected anaerobically through the septum after 10 min of illumination or dark incubation, and aliquots (300 μL) were drawn from the reaction cuvette. The aliquots were reduced with dithionite (50 mM). Each sample contained nNOS (5 μM) and NT (5 μM) in the presence of NOHA and BH_4 (1 mM), calmodulin (30 μM), and Ca^{II} (300 μM) in Tris buffer (50 mM) containing NaCl (150 mM) and glycerol (5%) at pH 7.5. Irradiation was performed at $\lambda = 400 \pm 30$ nm for 10 min. The figure represents the sum of two scans recorded at 77 K and 20 mW microwave power. The spectrometer settings are described in the text. A) NO·Fe^{II}·MGD complexes (300 ± 30 pmol) obtained after 10 min of illumination. B) Spectrum obtained after illumination in the absence of nNOS. C) Spectrum obtained in the presence of nNOS without illumination.

Photoinduced electron transfer from NT* to FAD

Fast optical absorption spectroscopy was used to study forward and backward electron transfer from the bound NT to FAD, together with the role of calmodulin in intramolecular electron flow in the reductase domain of the constitutive nNOS. Laser excitation was carried out at 405 nm. Figure S1 in the Supporting Information shows that, at this wavelength, about 50% of the photons promoted NT excitation, with some inner filter effects of the heme. The excited-state NT* presented a broad absorption band with a maximum at 620 to 670 nm, strongly red-shifted with respect to the ground state, with absorption peaking at 380 nm; this is consistent with considerable delocalization of the electrons along the polyenic linker (refs. [17, 24] and Figure 4). When associated with proteins unable to accept electrons from NT*, the decay of protein-bound NT* was found to be multiexponential. NT* decayed to zero within $\tau_3 = 400 \pm 60$ ps.[17] When NT was bound to the reductase domain of eNOS, the rate of decay was enhanced to $\tau_3 = 110 \pm 26$ ps. Direct excitation of nNOS heme alone yielded a weak signal that decayed within 10 ps (Figure S2 in the Supporting Information).

1) Effect of Ca^{II}/calmodulin on photoinduced electron transfer from NT to FAD in NT-bound WT nNOS*: The absorption decay of NT* bound to nNOS after laser excitation at 405 nm, with probing at 613 nm, is shown in Figure 4A. Data were obtained over three timescales to obtain a reliable asymptotic value. The decay of nNOS-bound NT* was found to be multiexponential over the ps to ns time range[17] (Table 1) in the absence of Ca^{II}/calmodulin [CaM (−)]. The first phase was best fitted by $\tau_1 = 1.4 \pm 0.3$ ps (34%) and $\tau_2 = 8.7 \pm 1.5$ ps (16%). The second phase was observed in the range of hundreds of ps and was fitted by two components: $\tau_3 = 104 \pm 15$ ps and $\tau_4 = 280 \pm 40$ ps, leveling off at a small, non-zero asymptotic value. NT decay in the full-length CaM (−) nNOS protein was thus similar to that observed in the presence of the eNOS reductase domain, characterized by $\tau_3 = 94 \pm 10$ ps and $\tau_4 = 234 \pm 40$ ps (Table 2 and ref. [17]).

The presence of Ca^{II}/calmodulin [CaM (+)] bound to nNOS had a significant effect on the kinetics of NT* decay (Figure 4A and Table 1). Firstly, the amplitude A_1 of the fastest picosecond component decreased from 0.34 to 0.20 and the amplitude A_2 dropped from 0.16 to a negligible value. Secondly, lifetime τ_3 was decreased from 104 ± 15 ps [CaM (−)] to 21 ± 3 ps [CaM (+)], whereas for the slowest process, τ_4 increased from 280 ± 40 ps to $\tau_4 = 500 \pm 80$ ps under CaM (−) and CaM (+) conditions, respectively. The relative weight A_4 of the slowest process increased from 0.20 [CaM (−)] to 0.43 [CaM (+)]. The asymptotic value was significantly increased by the presence of CaM (Table 1).

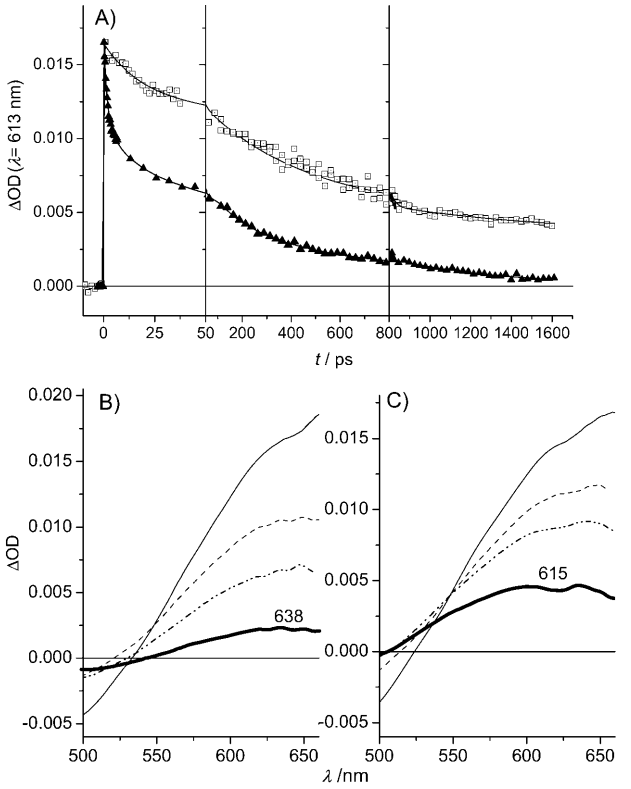

Figure 4. Effect of Ca^{II}/calmodulin binding to nNOS on the decay of NT* bound to the protein. A) Faster (crude) decay (monitored at 613 nm) of nNOS-bound NT* was observed in the absence of Ca^{II}/calmodulin (1 mM/250 μM (▲) than in its presence (□). [nNOS] = [NT] = 35 μM, [NOHA] = 2 mM, [BH_4] = 1 mM in Tris buffer (pH 7.5, 50 mM) containing NaCl (150 mM) and glycerol (5%, *v/v*). The lines represent the best fit to the data (Table 1). Note the much larger asymptotic values in the presence of CaM [CaM (+)] than in its absence [CaM (−)]. B), C) Comparison of the transient spectra of NT bound to nNOS with/without CaM (from a single experiment and accumulation of ten scans). B) NT bound to nNOS without calmodulin [CaM (−)] at 18 °C. C) NT bound to nNOS in the presence of CaM. t = 15, 100, 300, and 800 ps as shown by the solid, dashed, dashed-dotted and bold full lines, respectively. The experimental conditions in (B) and (C) are similar to those used in (A).

2) Transient absorption spectra: The observed kinetics depended largely on the presence or absence of Ca^{II}/calmodulin bound to nNOS. In the absence of CaM, the transient spectrum obtained at 15 ps presented a maximum at ≈642 nm, slightly blue-shifted to 638 nm at 100, 300, and 800 ps (Figure 4B). Under CaM (+) conditions, the spectrum obtained at 15 ps was similar that obtained in the absence of CaM. However, a broad maximum at ≈615 nm was recorded at 800 ps (Figure 4C). We attribute this broadening of the spectrum to a transient species specifically requiring the presence of CaM.

Figure 5A shows absorption at t = 800 ps in the presence of CaM and details the calculated spectra of the oxidized NT and reduced FAD species used in the fit.[17,24] A reasonable fit of the broad positive band centered at about 615 nm and accounting for both the oxidized NT species and FADH°−FAD absorption was compatible with the transformation of FAD to FADH° and of NT to the oxidized NT species composed of 60 ± 10% of NT^+ and 40 ± 10% of NT^{2+} at 18 °C. Some discrepancies between measured and calculated absorption at ≈510 nm remain. The broad absorption band between ≈530 and 640 nm suggested that transient formation of the "blue semiquinone" FADH° was occurring, with $\Delta\varepsilon_{613}$(FADH°−FAD) = 3.2 × 10^3 M^{-1}cm^{-1}.[21,26] Note the major contributions of NT^+ and NT^{2+}: $\varepsilon_{613} = 2.7 \times 10^4$ and 2.1×10^4 M^{-1}cm^{-1}, respectively. At 482 nm, the relative absorption of FADH°−FAD prevailed and $\Delta\varepsilon_{482}$(FADH°−FAD) = -8.5×10^3 M^{-1}cm^{-1}, with $\varepsilon(NT^+) = 0$ and $\varepsilon(NT^{2+}) = 5.3 \times 10^3$ M^{-1}cm^{-1}, approximately reproduced by the fit.

Figure 5B shows the smaller amplitude of the transient spectrum obtained with CaM (−) samples at t = 800 ps. This absorption spectrum is consistent with the transformation of FAD to reduced and unprotonated FAD^- and the superimposition of 60 ± 10% of NT^+ and 40 ± 10% of NT^{2+}. The fit corresponded to the contributions of the oxidized NT^+ and NT^{2+} species identical to those under CaM (+) conditions (Figure 5A) but assumed that the anionic (unprotonated) reduced flavin FAD^- was the redox partner, with the difference spectrum shown in Figure 5B. Absorbance at 450–480 nm and in the 550–630 nm range is sensitive to the protonation state of the reduced flavin, with $\Delta\varepsilon_{613}(FAD^- - FAD) = 0$ and $\Delta\varepsilon_{482}(FAD^- - FAD) = -4.6 \times 10^3$ M^{-1}cm^{-1}. These differences between CaM (+) and CaM (−) accounted for the absorption maximum at ≈635 nm and the smaller minimum in the 455–482 nm range in Figure 5B relative to Figure 5A. Uncertainty at 455-482 nm was greater under CaM (−) conditions than under CaM (+) conditions, due to the smaller residual signal (ΔOD ≈ 7×10^{-4}).

The observed spectral changes in the range of hundreds of ps appear to be fully consistent with the expected sequence: i) photoexcitation of NT to generate NT* [Eq. (1)], ii) electron

Table 1. Kinetic parameters of nNOS-bound NT decay in the presence or in the absence of Ca^{II}/calmodulin.

Enzyme	CaM	λ [nm][a]/ SVD analysis	τ_1[b] [ps]	A_1	τ_2* [ps]	A_2	τ_3* [ps]	A_3	τ_4* [ps]	A_4	A_5
WT nNOS	−	613	1.4	0.34	8.7	0.16	104	0.25	280	0.20	0.05
	−	SVD1	1.2	0.33	10.0	0.15	92	0.25	333	0.19	0.08
WT nNOS	+	613	2.5	0.20			21	0.13	496	0.43	0.24
	+	SVD1	1.7	0.10			20	0.21	526	0.48	0.21
S1176T	+	613	2.1	0.20			34	0.20	567	0.55	0.05
S1176A	+	613	3.2	0.12			38	0.17	507	0.22	0.49

[Enzyme] = [NT] = 30–50 μM in the presence of CaM (5 equiv) as specified. [BH_4] = [NOHA] = 1 mM. [a] Single-wavelength fit of the crude data at λ = 613 nm or by SVD analysis; the presented fit corresponds to the main SVD component. [b] The errors are: $\tau_1 \pm 0.3$ ps, *$\tau_2 \pm 2$ ps, $\tau_3 \pm 25$ ps [CaM (−)] and ± 5 ps [CaM (+)], $\tau_4 \pm 50$ ps.

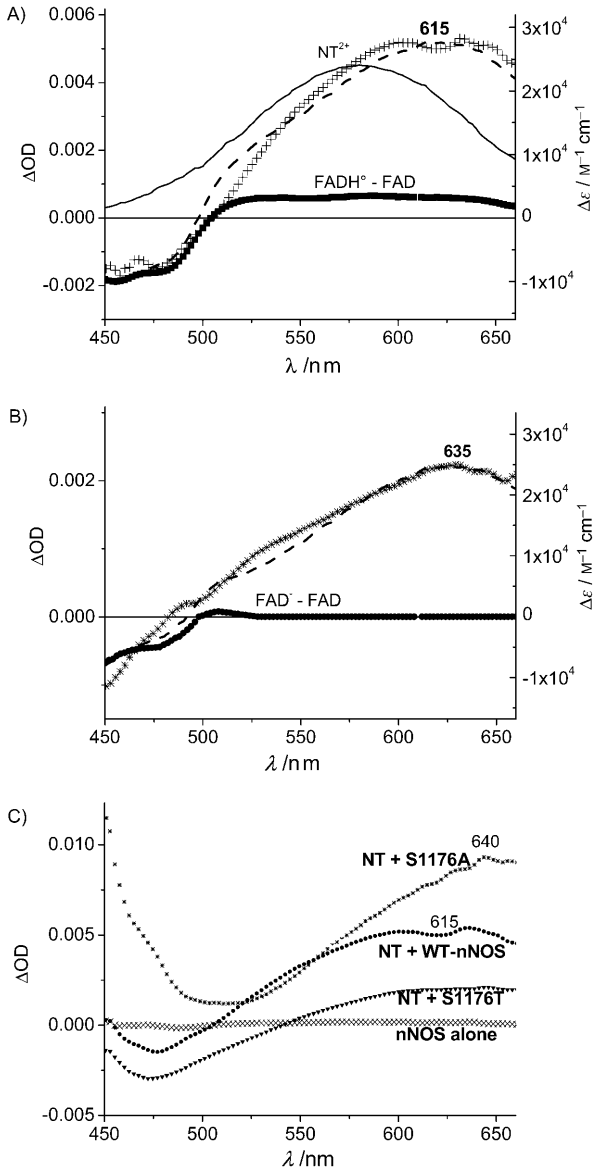

Figure 5. Fit of the transient spectra recorded at $t = 800$ ps in A) CaM (+) WT nNOS and in B) CaM (−) nNOS WT in the presence of NT. In both cases the oxidized NT species were NT^+ (60%)+NT^{2+} (40%), corrected for the bleaching of NT, and the fit (-----) assumes that the reduced FAD was protonated ($FADH^\circ$) in A) [CaM (+)] but unprotonated in B) [CaM (−)]. The calculated difference spectrum of $FADH^\circ - FAD^-$ (■) and NT^{2+} (——) are shown in (A) (NT^+ is omitted for clarity), whereas the calculated difference spectrum $FAD^- -$ FAD is shown in (B). The experimental points (+ for A) and * for B)) represent the means of two and four experiments in A) and B), respectively; see legend of Figure 4 A for experimental conditions. C) Effect of S1176 mutagenesis on the transient spectrum of NT bound to CaM (+)-nNOS at $t =$ 800 ps. ● (WT), ▼ (S1176T), * (S1176A), × nNOS without NT.

transfer from NT* to FAD [Eq. (2)], and iii) protonation of FAD^- to $FADH^\circ$ [Eq. (3)], in competition with iv) charge recombination [Eq. (4)]. Scheme 2 shows the detailed sequence for the productive NO pathway in CaM (+) samples.

$$NT + h\nu \rightarrow NT^* \quad (1)$$

$$NT^* \rightarrow NT + h\nu' \ (+\Delta) \quad (1')$$

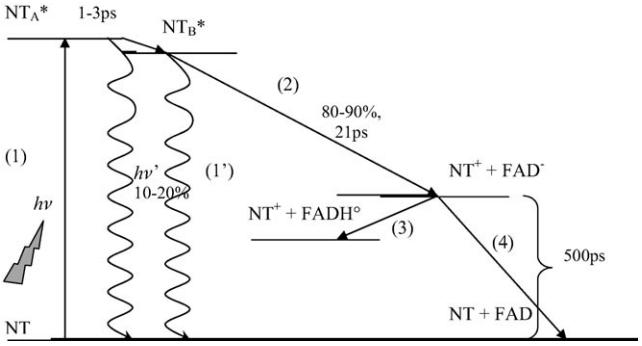

Scheme 2. Proposed decay pathway of the excited NT bound to the CaM (+)-nNOS protein based on ultrafast kinetics: Excitation at 405 nm promotes the formation of a first excited Franck–Condon state of NT (NT_A*), which decays to a second (possibly solvent-relaxed) excited state (NT_B*), accounting for the fast shift of the transient maximum within a few ps. Fluorescence emission from these states was assessed by following the decay of the stimulated emission at ≈500 nm. About 80% of NT_B* species transferred an electron to FAD, yielding NT^+ and FAD^- within 21 ps.[2] This (ground state) charge-separated state may then recombine to the ground state [Eq. (4)] or convert to another state in which FAD^- is protonated [Eq. (3)]. Recombination may proceed between $FADH^\circ$ and NT^+ at a later stage [Eq. (6)]. The net escape (charge separation) amounts to ≈20%, and is ultimately used for NO formation [Eqs. (5), (7), and (8)]. The doubly oxidized nanotrigger (NT^{2+}) may be obtained through consecutive ET, either by a thermal process when released into the solution (reflecting the rate of NT dissociation from the protein) or by a photoinduced processes [Eqs. (5) or (5′)].

(unproductive deactivation pathways)

$$NT^* + FAD \rightarrow NT^+ + FAD^- \ (k_{ET}) \quad (2)$$

$$FAD^- + H^+ \rightleftharpoons FADH^\circ \ (k_H) \quad (3)$$

$$NT^+ + FAD^- \rightarrow NT + FAD \ (k_b) \quad (4)$$

$$NT^* + FADH^\circ + H^+ \rightarrow NT^+ + FADH_2 \quad (5)$$

$$NT^{+}* + FADH^\circ + H^+ \rightarrow NT^{2+} + FADH_2 \quad (5')$$

$$NT^+ + FAD^- \rightarrow NT + FADH^\circ + H^+ \ (k'_b) \quad (6)$$

$$FADH_2 + FMN \rightleftharpoons FADH^\circ + FMNH^\circ \rightleftharpoons FAD + FMNH_2 \quad (7)$$

$$FMNH_2 + Fe^{III}\ (\text{heme})\text{-NOHA} + O_2 \rightarrow FMNH^\circ + Fe^{III} + NO + \text{citrulline} + H_2O \quad (8)$$

The sequence (1)–(2), taking place over ps, yielded photoinduced electron injection from NT* to FAD (τ_3), with unproductive relaxations globally accounted for by Equation (1′). The decay over hundreds of ps (τ_4) corresponded to: $k_{obs} = k_b + k_H$, where k_b and k_H represent the rate of backward electron transfer [Eq. (4)] and the rate of FAD^- protonation (assumed to be faster than its deprotonation), respectively. Calmodulin increased the rate of FAD^- protonation (Figure 5). This resulted in a slower rate of backward electron transfer with partial switching from Equation (4) to Equation (3) under CaM (+) conditions, while charge recombination occurred exclusively as shown in Equation (4) under CaM (−) conditions. The relative weights of Equations (4) and (3) were estimated by calculating the relative ratio $((A_4 + A_5)/A_5)$:$([FAD^-] + [FADH^\circ])/[FADH^\circ] \approx (A_4 + A_5)/A_5 = k_{obs}/k_H$ and $k_{obs} = k_b + k_H$.

Given the k_{obs} values for nNOS WT [CaM (+)] (Table 2) and $(A_4+A_5)/A_5 \approx 3$, one can extract the values of k_H and k_b as $k_H = (7+3)\times10^9$ and $k_b = (1.3+0.4)\times10^9\ s^{-1}$. Thus, in the presence of Ca^{II}/calmodulin, protonation (k_H) competes with charge recombination (k_b). In eNOSred or nNOS in the absence of CaM, no protonation occurred ($k_{obs} = k_b = 3\times10^9\ s^{-1}$).

Table 2. Calculated rates of electron transfer (k_{ET}) from NT* to FAD and of observed charge recombination (k_{obs}) based on $k_N = 2.0\times10^9\ s^{-1}$.[17]

Sample	k_{ET} [s^{-1}]	k_{obs} [s^{-1}][a]	$R = k_{ET}/k_{obs}$
nNOS WT [CaM (+)]	$(4.6\pm0.8)\times10^{10}$	$(2.0\pm0.4)\times10^9$	23
nNOS WT [CaM (−)]	$(1.1\pm0.4)\times10^{10}$	$(3\pm1)\times10^9$	3.7
eNOSred [CaM (−)]	$(7\pm2)\times10^9$ [17]	$(4\pm1)\times10^9$	1.8
nNOS S1176T [CaM (+)]	$(2.7\pm0.5)\times10^{10}$	$(1.8\pm0.5)\times10^9$	15

[a] k_{obs} is the observed rate of decay in the range of hundreds of ps. In CaM (+) proteins, $k_{obs} = k_b + k_H$, where k_H is the rate of FAD^- protonation (promoted by CaM binding) and k_b is the rate of recombination of $NT^+ + FAD^-$ [Eq. (4)] in CaM (−). $k_{obs} = k_b$, the rate of $NT^+ + FAD^-$ backward electron transfer.

The optical data did not identify the source of the proton involved in this mechanism. The NT injects electrons but cannot provide the proton from NT^+; only NT^{2+} would be able to donate a proton from its iminium NH_2^+ terminal. NT^{2+} could be obtained in solution through NT^+ release (k_{off}) and subsequent disproportionation.[24] In addition, NT* (or possibly NT^{+}*) could donate a second electron to $FADH^\circ$ to produce $FADH_2$ [Eqs. (5) or (5′)] once these species accumulated as shown in Equation (3). Experimental evidence for these processes would require the longer timescales achievable with a ns setup.

The source of the proton, assumed to be provided by the protein, was investigated by two complementary approaches. In the first one, molecular modeling was used to screen potential candidates that might transfer a proton to FAD^- in the NADPH·nNOS complex (Figure 2). The Ser1176 residue was identified by molecular modeling as a potential participant in FAD^- protonation. It is located close both to the NH_2 terminal of NT and to the FAD isoalloxazine ring (Scheme 1). It belongs to the catalytic triad and is H-bonded to Cys1349 and Asp1393 and is also located close to a water molecule present in the X-ray structure.[8–12] We therefore studied the kinetics of $FADH^\circ$ formation in the Ser1176A and Ser1176T mutants of nNOS in a second experimental approach.

3) Role of Ser1176 in NT-induced electron transfer to FAD*: An increase in the FMN fluorescence of Ser1176A and Ser1176T provided evidence for similar binding of NT both to the two mutants and to WT nNOS (Figure 1 and data not shown). Figure 5C compares the transient spectra recorded 800 ps after the pump when NT is bound to WT-nNOS and to the S1176T and S1176A mutants. S1176A displayed a marked difference, with the transient peaking at ≈640 nm, whereas the spectrum of S1176T was similar to that observed with WT nNOS. Note the similar maximum obtained with S1176A at 640 nm and the spectrum recorded with WT nNOS CaM (−), peaking at 635–638 nm.

These spectral differences paralleled the marked changes in kinetics shown in Table 1 and Figure S3 in the Supporting Information. The S1176T point mutation considerably increased decay amplitude to hundreds of ps and decreased the asymptotic value, whereas the S1176A mutation had the opposite effect on decay: A_4 was 0.43 (WT), 0.55 (S1176T), and 0.22 (S1176A). Accordingly, as the asymptotic value A_5 varied from 0.24 (WT) to 0.05 (S1176T) and 0.49 (S1176A), the ns decay was strongest for the threonine mutant and weakest for the alanine mutant. This suggests that at least some of the decay over the range of hundreds of ps to ns depends on the H-bonding properties of Ser1176.

Discussion

1) NT selectively targeted nNOS and its photoactivation led to formation of the catalytic product NO

NOS catalysis is driven by the consumption of NADPH and involves the transfer of a hydride from NADPH to FAD. This process is tightly regulated by a conformational change, requiring the rotation of the Nic moiety of NADPH (see movie obtained by molecular modeling in the Supporting Information) and the tilting of Phe1395 to allow access to FAD at a correct distance and in the correct conformation for electron transfer. In this work, we used a NT bound to the NADPH site of the constitutive full-length nNOS enzyme to initiate the first step of catalysis with light (Scheme 1). The selective targeting of NT to nNOS was demonstrated by molecular modeling (see below) and fluorescence spectroscopy. The emission binding modes at 465 nm were similar for NT and for $NADP^+$-bound to nNOS. However, the NADPH·nNOS complex was not easily disrupted by calmodulin binding, unlike the complex with the natural cofactor, suggesting that the NADPH–nNOS complex was more stable than the NADPH·nNOS complex. Consistent with these findings, our previous stopped-flow data showed that NT had a greater affinity than NADPH for the eNOS reductase domain.

Simulations showed that the active form of NADPH for hydride transfer and NT share many binding similarities. NT was docked in the NADPH site by multiple H-bonds to the nucleotide part of the molecule. As would be expected from its design, NT interacted with Arg1400, Arg1314, Ser1313, and Arg1284, as observed for both active and inactive NADPH structures.[9,18] Additional H-bonding interactions anchored the NH_2 terminal of NT to the protein; the van der Waals binding energy of the NT chromophore was found to be similar to that of the Nic moiety of active NADPH. Moreover, the distance between the active redox groups and FAD were similar in active NADPH and NT, but strikingly different from that in the inactive form of NADPH. This difference is reminiscent of the "straight" NADPH conformation found in some X-ray structures, as opposed to the "folded" inactive conformation in other NADPH-binding proteins structures as in the case of nNOS.[27] For the FAD to be accessible to active NADPH, the Phe1395 residue must rotate away from FAD. This release of the Phe1395 conformational lock is readily achieved upon NT binding. The semirigid conjugated linker between the two amine (donor)

groups, together with the amide linker connecting the chromophore and nucleotide part of the NT, played a major role in generating the straight conformation of NT required for the rapid triggering of photoinduced electron injection. Molecular modeling and fluorescence spectroscopy strongly suggested that the NT likely probed an environment similar to that probed by active NADPH in the nNOS enzyme.

The NT also drove the catalysis up to NO formation, just like NADPH. The NT induced the formation of the ferrous nitrosylated complex in nNOS, as shown by absorption difference spectroscopy, provided that CaM was present, but no ferrous nitrosylated complex was detected in CaM (−)-nNOS samples.[17] NO spin-trapping showed that NT irradiation induced a relative increase in NO yield over that obtained with NADPH, estimated to be three to four times basal NO levels after correction for the 50% light absorption by the NT. This enhancement was obtained with a NT/nNOS stoichiometry of 1:1, whereas the production of basal NO levels required excess NADPH (mM concentrations). The initial catalytic cycles therefore run at least as efficiently as under basal conditions and more likely are enhanced by NT photoactivation, which may be particularly relevant for future cellular applications (Scheme 1).

2) Calmodulin promotes electron flow during the initiation of nNOS catalysis

NT photoactivation made it possible to exert precise temporal control over the initiation of nNOS catalysis, as demonstrated by ultrafast transient absorption measurements. NT excitation with the laser pump promoted the formation of an excited state (NT*). At the excitation wavelength, 50% of the photons at 405 nm were absorbed by the heme of the protein, but yielded a negligible transient signal ($\Delta OD \leq 5\times10^{-4}$) after $\approx$10 ps (Figure S2 in the Supporting Information).

The decay of NT* within nNOS generated a first short-lived species (τ_1 = 1–3 ps), possibly due to vibrational cooling. The second lifetime of NT was significantly shorter for nNOS-CaM (−) and the eNOS reductase domain [$\tau_2 = 8.7\pm1.5$ ps and 7 ± 2 ps respectively, versus $\tau_2 = 20\pm4$ ps in Phe1160Ala (equivalent to Phe1395Ala in nNOS).[17] This lifetime corresponded to an excited state complex (NT·Phe)* for a minor population ($\approx$10%).[17] It was not observed in the presence of Ca^{II}/calmodulin binding, which suggested that Phe1395 was completely tilted away under these conditions (Table 1), consistently with the molecular modeling data (Figure 2). Thus, NT bypassed the conformational regulation of Phe1395, blocking access to FAD.

The third lifetimes were similar in NT bound to the CaM-depleted nNOS and in the eNOS reductase domain ($\tau_3 = 96\pm10$ ps and $\tau_3 = 110\pm26$ ps, respectively).[17] The corresponding NT lifetime in the absence of ET was $\tau_3 = 400\pm60$ ps. The rates of electron transfer were thus similar, within experimental error, in the two cases: $k_{ET} = (1.0\pm0.3)\times10^{10}\ s^{-1}$, based on $k_N = 2\times10^9\ s^{-1}$, k_N being the rate of natural decay. In the presence of Ca^{II}/calmodulin binding, NT* decay was shorter ($\tau_3 = 21\pm3$ ps). The rate of electron transfer was found to be $k_{ET} = (4.6\pm0.8)\times10^{10}\ s^{-1}$ in nNOS (estimates produced by use of the Marcus equation suggested that the NT*–FAD distance became closer by 0.53 Å in CaM (+) nNOS relative to CAM (−) assuming $\lambda = 0.7$ eV, $\beta = 1.1\ Å^{-1}$;[28] Table 1). Calmodulin binding thus increased the rate of NT*-induced electron transfer by a factor of four [Eq. (2) and Scheme 2]. A stoichiometric ratio of 1:1 NT/NADPH site in nNOS is required for this ET process to take place.[29]

Figure 4 shows the slower decays observed for the longest lifetimes and higher asymptotic values in the presence of CaM. These absorption changes occurred after electron transfer, and this step was therefore attributed to a reaction between ground-state species. The highly exergonic electron transfer between the oxidized NT^+ and the reduced flavin [Eq. (4)] contributed to this decay. Indeed, for efficient electron flow in nNOS, charge recombination must be slowed down. The presence of CaM resulted in a slowing of the rate of charge recombination (in the hundreds of ps). The increase in the asymptotic value accounted for the greater yield of ns charge separation with CaM (Figure 4A). The fit of the associated transient spectra at 800 ps suggested that CaM enhanced FAD^- protonation (Figure 5). Thus, two main decay pathways accounted for the observed τ_4 lifetimes in WT nNOS (Scheme 2): the faster process [Eq. (4)] is the backward electron transfer between FAD^- and NT^+, the main recombination pathway in CaM (−) samples, with only 5–8% charge separation on the ns timescale (Table 1). The competing processes in CaM (+) samples involved FAD^- protonation [Eq. (3)], increasing the charge separation between $FADH^\circ$ and NT^+ to a value of 20 to −30% (Scheme 2). A protonation rate of $k_H = (7\pm3)\times10^8\ s^{-1}$ was estimated from the ns data for WT nNOS CaM (+), whereas a rate of only $k_H = (1.6\pm0.5)\times10^8\ s^{-1}$ was obtained for the S1176T mutant. Indeed, molecular modeling identified Ser1176, which is located close both to the NT terminal amine (3.1 Å) and to FAD (3.0 Å), as a residue assisting in FAD protonation, together with its H-bonding partners (8). Ser1176, through its hydrogen bonds, may lower the pK_a of the neighboring water molecule(s) (Scheme 1). Consistently with this hypothesis, S1176A could not form these H-bonds and no FAD^- protonation was observed in the transient spectra. In contrast, S1176T was still able to form a single hydrogen bond and some FAD^- protonation was still detected (Figure 5C). Our data are consistent with the reported 20-fold decrease in nNOS flavin reduction rate seen on the mutation of Ser1176 to Ala. Moreover, the effect of calmodulin on nNOS activity was greatly reduced by this mutation.[12]

We estimated that FAD^- protonation decreased the rate of charge recombination, at least from $k_b = (3\pm1)\times10^9\ s^{-1}$ to $k_{b'} < (7\pm3)\times10^8\ s^{-1}$ in WT nNOS CaM (+). Alternatively, an increase in the distance between NT^+ and FAD^- induced by a structural change may have occurred in the range of hundred of ps in CaM (+) samples, accounting for the decrease in recombination rate. However, this seems unlikely as it cannot account for the protonation of FAD^- deduced from the CaM (+) transient spectra.

Electron flow was estimated by determining the ratio (R) of the forward electron transfer rate (k_{ET}) to the observed decay

(by charge recombination as in Equation (4) in CaM (−) or by formation of $FADH^{\circ}$ via Equations (3) and (4) in CaM (+)). CaM binding increased this ratio by a factor of 6.2, from $R = 3.7$ to 23 (Table 2).

The 1–2 ns decay in WT nNOS was strongly affected by the presence of CaM (Figure 4). This may reflect the formation of $FMNH^{\circ}$ by interflavin electron transfer, enhanced by CaM. Interestingly, the S1176A mutant hardly decayed between 800 ps and 1.6 ns, unlike the S1176T mutant. We attribute the lack of decay of the S1176A mutant to the instability of FAD^{-}, as previously reported.[12] FAD^{-} decay should take place within ≈300 ps to account for the lower level of back electron transfer in this mutant (Figure S3 in the Supporting Information and Table 2). Moreover, the S1176A mutant has a significantly higher FMN redox potential (>40 mV) than S1176T and WT nNOS (−120 mV).[12] This may account for the lack of back electron transfer in S1176A. Alternatively, Panda et al. have suggested that there may be a conformational change in the FAD environment gating interflavin electron transfer, consistently with the slow 1–2 ns process reported here.[12] Indeed, the C-terminal tail lies at the interface between the FAD and FMN binding domains and interacts with the auto-regulatory region (AR) when NADPH is bound. Calmodulin binding altered the position of the tail, releasing the interaction with AR through the subsequent movement of FMN in an intermediate state.[12]

We performed independent fluorescence experiments to distinguish between these two hypotheses. Flavins display strong fluorescence in the oxidized state, and this fluorescence is quenched upon reduction. The fluorescence lifetime of free FMN in buffer is ≈4 ns.[30] If the interflavin FAD to FMN ET took place within 1–2 ns, then FMN fluorescence should be quenched and steady-state fluorescence by FMN suppressed. Instead, calmodulin binding increased FMN fluorescence intensity by 25% in NT-bound nNOS, whereas this fluorescence decreased in nNOS with $NADP^{+}$ (Figure 1). It is therefore highly unlikely that $FMNH^{\circ}$ is formed within 1 to 2 ns. Our data suggest that a conformational change in the immediate vicinity of $FADH^{\circ}$ may be a prerequisite for interflavin ET. This structural change was found to be crucially dependent on the presence of calmodulin and the integrity of H-bonds between FAD and the catalytic residues S1176 and Asp1393. S1176T can still form a hydrogen bond with Asp1393, whereas this bond is not formed in the alanine mutant.[12] Our absorption decays at 613 nm do not rule out the possibility of a second electron transfer through NT* (or NT^{+}*) as in Equation (5) within 1 to 2 ns, producing $FADH_2$ in addition to the conformational change involving $FADH^{\circ}$ suggested above.

Overall, our data show that calmodulin enhanced electron flow by increasing forward electron transfer to FAD and promoting proton transfer to FAD^{-}. This slowed down back electron transfer and increased the net electron flux towards FMN. Calmodulin therefore increased catalytic efficiency. Our data suggest that FAD is reduced in a fast pathway including a sequential one-electron, one-proton transfer and one-electron transfer. A similar pathway has recently been proposed to take place in ferrodoxin reductase from *Pseudomonas aeruginosa*, in which the C4 atom of Nic and the N5 atom of FAD are 15 Å apart, and in horseradish peroxidase; moreover, a NADH analogue reacted through an ET pathway rather than direct hydride transfer.[31–33]

The timescale of interflavin electron transfer was reported to extend over more than a few ns.[22] This is very slow in view of the short interflavin distance and the favorable ΔG value of −100 mV.[16] The slow nature of this transfer reaction is confirmed by our own observations of FMN fluorescence. It suggests that interflavin transfer requires a conformational change either in the C-terminal tail or in FMN itself, as suggested by Panda et al.[12]

Conclusions

Significance and perspectives for synchronized enzymatic catalysis

Pulsed light excitation of the NT initiated the enzyme catalytic cycle and provided us with a convenient means of synchronizing an ensemble of proteins in solution with a femtosecond laser pulse. Synchronization is achieved on a significantly longer timescale than the pulse width, as determined by the rate of electron transfer into the flavin domain. For NT bound to CaM (+) nNOS, electron transfer took place in ≈20 ps. This timescale is likely to be affected by parameters affecting ET rates. For example, the removal of calmodulin increased the timescale for synchronization of the action of the constitutive NO synthase nNOS, to ≈100 ps. This synchronization provides an alternative to single-molecule techniques for the targeting and control of biochemical redox processes. It is based principally on correct targeting of the narrow NADPH site, while a semirigid conformation is maintained. This blocks the enzyme in an active conformation (by moving Phe1395 away from FAD), making it possible to study fast electron-transfer processes. The NT thus constitutes a powerful mechanistic tool, making it possible to identify steps under kinetic control with a trigger, on picosecond timescales. This tool may be particularly useful for time-resolved X-ray studies and for the design of specific activators or inhibitors of enzymatic activities. Our EPR data showed that the activation by light of protein-bound NT resulted in the release of NO radicals from NOHA. This property may be exploited to control and localize the release of free NO in cells with high spatial and temporal resolution by two-photon excitation (Scheme 1).[17,24,29] We are currently working along these lines and investigating the possible extension of the NT concept to other flavonoid proteins.

Experimental Section

Materials: L-Arginine, (6*R*)-5,6,7,8-tetrahydrobiopterin (BH_4), calmodulin, Tris buffer, *N*-hydroxyarginine (NOHA), potassium ferricyanide, and glycerol were purchased from Sigma. High-purity argon (99.9995%) was obtained from Air Products. Full-length nNOS was overexpressed in *E. coli* and purified as previously described.[34] Site-directed mutagenesis at position S1176 was performed as previously described.[12]

Time-resolved spectroscopy: Pulsed light excitation at a rate of 500 Hz was achieved with a home-built TiSa oscillator and a 1 kHz regenerative amplifier (Spitfire, Spectra Physics). The 810 nm light pulses each had a power of 0.5 mJ and lasted 50 fs.[17] The beam was separated into pump and probe. Pump pulses centered at 405 nm were generated with a 0.5 mm BBO crystal used in SHG configuration. White light probe pulses in the 430 to 700 nm range were generated by focusing part of the fundamental on a CaF_2 window and separated into test and reference beams. The sample was positioned away from the focal point and the intensity of the pump beam was reduced with neutral density filters, thus avoiding white light continuum generation in the sample. The beams each had a diameter of 150 μm and pump energy of about to 2 μJ at the sample position. These beams, after passing through the sample, were dispersed and detected shot-by-shot on a CCD camera configured as a dual-array detector. The sample was renewed between subsequent pulse pairs by rotation perpendicular to the beams. The signal-to-noise ratio was improved by accumulation of ten wavelength scans in two time windows: 1–50 ps and 50–800 ps or 1–10 ps and 10–200 ps. To obtain delay times longer than 800 ps between pump and probe beams (Figures 4 and S2 in the Supporting Information), the probe was delayed by 12.2 cm with mirrors. The signal was optimized at 613 nm by use of MbCO as a reference. Carbon monoxide bound to reduced myoglobin was monitored under the same conditions and used as a reference for an undecaying signal over the time scales of 200 to 800 ps and up to 1.6 ns. Data were analyzed by singular value decomposition (SVD) of the time–wavelength matrix and by single wavelength fits to the raw data.

Molecular dynamics simulations: Molecular dynamics modeling was carried out with the CHARMM 33 software.[35] The calculations used the PDB file 1TLL,[9] with the missing residues 740–742, 831–835, 850–871, 952–958, and 1414–1429 (chain A) and 742–751, 830–839, 847–876, 953–958, and 1414–1429 (chain B) computer-generated and subjected to energy minimization before insertion into the final structure. The model consists of two identical chains of 665 residues each and contains two FAD and FMN moieties. Known water molecules from the X-ray structure (223) and a "box" of 5372 water molecules were added to the polypeptide chains. Hydrogen atoms were generated by use of the CHARMM HBUILD command. NT was introduced into the structure of the nNOS reductase by replacement of the natural NADPH cofactor. The common adenosine docking moiety was used to initiate chromophore construction with the "IC BUILD" CHARMM command. The energy of the structure was minimized with 200 SD and 2500 ABNR algorithm steps. A relative dielectric constant of one was applied to the entire structure. Motion equations were numerically integrated by use of the Verlet algorithm with 1 fs time steps. The following simulation protocol was used: heating from 0 to 600 K over 60 ps, equilibration phase at a constant temperature of 600 K over 100 ps, cooling from 600 K to 0 K over 60 ps, followed by a 2500-step ABNR energy minimization of the NT·nNOSred complex. Simulation with the NADPH cofactor was based on the following protocol: heating from 0 to 400 K over 80 ps, equilibration at 400 K for 1.5 ns, cooling from 400 K to 0 K over 160 ps, and energy minimization. The entire structure was saved at picosecond intervals for further analysis.

Steady-state fluorescence: Fluorescence emission spectra were recorded on an Eclipse (Varian) spectrofluorimeter, fitted with a thermostated cell holder, with use of aerated solutions placed in micro-cuvettes (60 μL). The emission spectra were recorded with excitation and emission slits set at $\Delta\lambda_{ex} = 10$ nm and $\Delta\lambda_{em} = 5$ nm, respectively.

NT-induced NO formation detected by EPR spectroscopy: A solution of nNOS (5 μM) was equilibrated with NOHA (1 mM), BH_4 (1 mM), calmodulin (20 μM), and Ca^{II} (100 μM) in Tris buffer (50 mM) at pH 7.5, NaCl (150 mM), and NT (5 μM) for 30 min on ice before the experiment. This aerated solution (750 μL) was transferred to a quartz cuvette and airtight with a rubber septum. This septum prevented the NO generated from escaping into the surrounding atmosphere. The cuvette was irradiated with a Xe lamp (150 W) passed through an optic fiber and filtered through a broad-band interference filter centered at 400 nm and a water filter to remove IR light. After 10 min of illumination, Fe·MGD complexes (0.4 mM, 100 μL) in Tris-buffer (pH 7.4, 100 mM) were injected into the cuvette.[25] An aliquot (300 μL) was extracted into a syringe through the septum and snap-frozen in liquid nitrogen. The yield of paramagnetic NO·Fe^{II}·MGD complexes in the aliquot was determined at 77 K with an EPR spectrometer (ESP300, Bruker, Rheinstetten, Germany) in an ER4103TM cavity with a quartz finger Dewar operating near 9.54 GHz. The apparatus setting was as follows: field modulation 5 G at 100 kHz, microwave power 20 mW, gain 2×10^5, time constant, and ADC conversion time 82 ms. At these settings, the detection limit for NO·Fe^{II}·MGD was $\approx$ 20 pmol. Trapping efficiency was estimated at 10%.

Acknowledgements

E.B. is supported by a fellowship from the French Ministère de la Recherche, A.S. acknowledges support by INSERM and the French National Research Agency ANR (ANR-08-PCVI-006), P.M. acknowledges financial support in the form of MSMT grants and from the Academy of Science of the Czech Republic (Grants # 0021620806 and KAN 200200651). S.P. acknowledges support in the form of a NIH Grant GM52419 (to Dr. Bettie Sue S. Masters, the Robert A. Welch Distinguished Professor in Chemistry at UTHSCSA, AQ0012). We thank Dr. Andras Lukacs for helpful discussions.

Keywords: emission spectroscopy · flavins · kinetics · metalloenzymes · molecular modeling · photocatalysis

[1] D. J. Stuehr, J. Santolini, Z. Q. Wang, C. C. Wei, S. Adak, *J. Biol. Chem.* **2004**, *279*, 36167–36170.
[2] C. S. Raman, P. Martasek, B. S. S. Masters, in *Porphyrin Handbook, Vol. 4* (Eds.: K. M. Kadish, K. M. Smith, E. Guilard), Academic Press, San Diego, **2000**, pp. 293–339.
[3] P. A. Hubbard, A. L. Shen, R. Paschke, C. B. Kasper, J. J. P. Kim, *J. Biol. Chem.* **2001**, *276*, 29163–29170.
[4] S. Daff, M. A. Noble, D. H. Craig, S. K. Chapman, A. W. Munro, S. Fujiwara, E. Rozhkova, I. Sagami, T. Shimizu, *Biochem. Soc. Trans.* **2001**, *29*, 147–152.
[5] P. F. Chen, K. K. Wu, *J. Biol. Chem.* **2003**, *278*, 52392–52400.
[6] D. H. Craig, S. K. Chapman, S. Daff, *J. Biol. Chem.* **2002**, *277*, 33987–33994.
[7] L. J. Roman, B. S. Masters, *J. Biol. Chem.* **2006**, *281*, 23111–23118.
[8] J. Zhang, P. Martasek, R. Paschke, T. Shea, B. S. Masters, J. J. P. Kim, *J. Biol. Chem.* **2001**, *276*, 37506–37513.
[9] E. D. Garcin, C. M. Bruns, S. J. Lloyd, D. J. Hosfield, M. Tiso, R. Gachhui, D. J. Stuehr, J. A. Tainer, E. D. Getzoff, *J. Biol. Chem.* **2004** *279*, 37918–37927.
[10] K. Panda, S. Adak, D. Konas, M. Sharma, D. J. Stuehr, *J. Biol. Chem.* **2004**, *279*, 18323–18333.

[11] D. Konas, N. Takaya, M. Sharma, D. J. Stuehr, *Biochemistry* **2006**, *45*, 12596–12609.
[12] S. P. Panda, Y. T. Gao, L. J. Roman, P. Martasek, J. C. Salerno, B. S. Masters, *J. Biol. Chem.* **2006**, *281*, 34246–34257.
[13] A. J. Dunford, K. R. Marshal, A. W. Munro, N. S. Scrutton, *Eur. J. Biochem.* **2004**, *271*, 2548–2560.
[14] D. W. Konas, K. Zhu, K. S. Aulak, G. W. Brudvig, D. J. Stuehr, *J. Biol. Chem.* **2004**, *279*, 35412–35425.
[15] C. Feng, G. Tollin, M. A. Holliday, C. Thomas, J. C. Salerno, J. H. Enemark, D. K. Ghosh, *Biochemistry* **2006**, *45*, 6354–6362.
[16] A. J. Dunford, S. E. Rigby, S. Hay, A. W. Munro, N. S. Scrutton, *Biochemistry* **2007**, *46*, 5018–5029.
[17] E. Beaumont , J. C. Lambry, C. Gautier, A. C. Robin, S. Gmouh, V. Berka, A. L. Tsai, M. Blanchard-Desce, A. Slama-Schwok, *J. Am. Chem. Soc.* **2007**, *129*, 2178–2186.
[18] M. Tiso, D. W. Konas, K. Panda, E. D. Garcin, M. Sharma, E. D. Getzoff, D. J. Stuehr, *J. Biol. Chem.* **2005**, *280*, 39208–39219.
[19] R. J. Jones, Y. T. Gao, T. M. Simone, J. C. Salerno, S. M. E. Smith, *Nitric Oxide* **2006**, *10*, 228–237.
[20] R. Gachhui, H. M. Abu-Soud, D. K. Ghosh, A. Presta, M. A. Blazing, B. Mayer, S. E. George, D. J. Stuehr, *J. Biol. Chem.* **1998**, *273*, 5451–5454.
[21] a) D. E. Pratt, V. Taiakina, J. G. Guillemette, *Biochim. Biophys. Acta Proteins Proteomics* **2007**, *1774*, 1351–1358; b) C. Feng, A. L. Dupont, N. J. Nahm, D. E. Spratt, J. T. Hazzard, J. B. Weinberg, J. G. Guillemette, G. Tollin, D. K. Ghosh, *J. Biol. Inorg. Chem.* **2009**, *14*, 133–142.
[22] Z. W. Guan, D. Kamatani, S. Kimura, T. Iyanagi, *J. Biol. Chem.* **2003**, *278*, 30859–30868.
[23] H. Matsuda, T. Iyanagi, *Biochim. Biophys. Acta Gen. Subj.* **1999**, *1473*, 345–355.
[24] A. C. Robin, S. Gmouh, O. Mongin, V. Jouikov, M. H. V. Werts, C. Gautier, A. Slama-Schwok, M. Blanchard-Desce, *Chem. Commun.* **2007**, 13 333–13 336.
[25] A. Vanin, E. E. H. van Faassen in *Electron Spin Resonance Spectroscopy, Biological Applications, in Encyclopedia of Analytical Science*, 2nd ed., Elsevier, **2005**.
[26] M. Du, H. C. Yeh, V. Berka, L. H. Wang, A. L. Tsai, *J. Biol. Chem.* **2003**, *278*, 6002–6011.
[27] O. Carugo, P. Argos, *Proteins Struct. Funct. Bioinf.* **1997**, *28*, 10–28.
[28] R. A. Marcus, N. Sutin, *Biochim. Biophys. Acta Rev. Bioenerg.* **1985**, *811*, 265–322.
[29] a) E. Beaumont , J. C. Lambry, A. C. Robin, P. Martasek, M. Blanchard-Desce, A. Slama-Schwok, *ChemPhysChem* **2008**, *9*, 2325–2331; b) E. Beaumont, J. C. Lambry, A. Slama-Schwok, unpublished results.
[30] P. van der Berg, A. van Hoek, A. J. W. G. Visser, *Biophys. J.* **2004**, *87*, 2577–2586.
[31] A. Wang, J. C. Rodriguez, H. Han, E. Schoenbrunn, M. Rivera, *Biochemistry* **2008**, *47*, 8080–8093.
[32] M. S. Afanayeva, M. B. Taraban, P. A. Purtov, T. V. Lashina, *J. Am. Chem. Soc.* **2006**, *128*, 8651–8658.
[33] J. Yuasa, S. Yamada, S. Fukuzumi, *J. Am. Chem. Soc.* **2008**, *130*, 5808–5820.
[34] L. Roman, E. Sheta, P. Martasek, S. S. Gross, Q. Liu, B. S. S. Masters, *Proc. Natl. Acad. Sci. USA* **1995**, *92*, 8428–8432.
[35] B. R. Brooks, R. E. Bruccoleri, B. D. Olafson, S. Swaminathan, M. Karplus, *J. Comput. Chem.* **1983**, *4*, 187–217.

Received: November 4, 2008
Published online on February 16, 2009

